PAPER

Impact of PET and MRI threshold-based tumor volume segmentation on patient-specific targeted radionuclide therapy dosimetry using CLR1404

To cite this article: Abigail E Besemer *et al* 2017 *Phys. Med. Biol.* **62** 6008

IOP Publishing | Institute of Physics and Engineering in Medicine Physics in Medicine & Biology

Phys. Med. Biol. **62** (2017) 6008–6025 https://doi.org/10.1088/1361-6560/aa716d

Impact of PET and MRI threshold-based tumor volume segmentation on patient-specific targeted radionuclide therapy dosimetry using CLR1404

Abigail E Besemer[1,2], Benjamin Titz[3], Joseph J Grudzinski[1], Jamey P Weichert[4], John S Kuo[2,5,6], H Ian Robins[2,7,8], Lance T Hall[4,5] and Bryan P Bednarz[1]

[1] Department of Medical Physics, University of Wisconsin-Madison, Madison, WI 53705, United States of America
[2] Department of Human Oncology, University of Wisconsin-Madison, Madison, WI 53705, United States of America
[3] OnLume Inc., 3300 Commercial Ave., Madison, WI 53714, United States of America
[4] Department of Radiology, University of Wisconsin-Madison, Madison, WI 53705, United States of America
[5] Carbone Cancer Center, University of Wisconsin-Madison, Madison, WI 53705, United States of America
[6] Department of Neurological Surgery, University of Wisconsin-Madison, Madison, WI 53705, United States of America
[7] Department of Medicine, University of Wisconsin-Madison, Madison, WI 53705, United States of America
[8] Department of Neurology, University of Wisconsin-Madison, Madison, WI 53705, United States of America

E-mail: bbednarz2@wisc.edu

Received 20 December 2016, revised 13 April 2017
Accepted for publication 5 May 2017
Published 6 July 2017

Abstract

Variations in tumor volume segmentation methods in targeted radionuclide therapy (TRT) may lead to dosimetric uncertainties. This work investigates the impact of PET and MRI threshold-based tumor segmentation on TRT dosimetry in patients with primary and metastatic brain tumors. In this study, PET/CT images of five brain cancer patients were acquired at 6, 24, and 48 h post-injection of ^{124}I-CLR1404. The tumor volume was segmented using two standardized uptake value (SUV) threshold levels, two tumor-to-background ratio (TBR) threshold levels, and a T1 Gadolinium-enhanced MRI threshold. The dice similarity coefficient (DSC), jaccard similarity coefficient (JSC),

and overlap volume (OV) metrics were calculated to compare differences in the MRI and PET contours. The therapeutic ^{131}I-CLR1404 voxel-level dose distribution was calculated from the ^{124}I-CLR1404 activity distribution using RAPID, a Geant4 Monte Carlo internal dosimetry platform. The TBR, SUV, and MRI tumor volumes ranged from 2.3–63.9 cc, 0.1–34.7 cc, and 0.4–11.8 cc, respectively. The average $\pm$ standard deviation (range) was 0.19 ± 0.13 (0.01–0.51), 0.30 ± 0.17 (0.03–0.67), and 0.75 ± 0.29 (0.05–1.00) for the JSC, DSC, and OV, respectively. The DSC and JSC values were small and the OV values were large for both the MRI-SUV and MRI-TBR combinations because the regions of PET uptake were generally larger than the MRI enhancement. Notable differences in the tumor dose volume histograms were observed for each patient. The mean (standard deviation) ^{131}I-CLR1404 tumor doses ranged from 0.28–1.75 Gy GBq^{-1} (0.07–0.37 Gy GBq^{-1}). The ratio of maximum-to-minimum mean doses for each patient ranged from 1.4–2.0. The tumor volume and the interpretation of the tumor dose is highly sensitive to the imaging modality, PET enhancement metric, and threshold level used for tumor volume segmentation. The large variations in tumor doses clearly demonstrate the need for standard protocols for multimodality tumor segmentation in TRT dosimetry.

Keywords: tumor segmentation, targeted radionuclide therapy (TRT), internal dosimetry, Monte Carlo, CLR1404, PET, MRI

(Some figures may appear in colour only in the online journal)

1. Introduction

Targeted radionuclide therapy (TRT) utilizes a radiolabeled cancer targeting molecular agent to preferentially deliver cytotoxic radiation to cancer cells throughout the body. Similar to chemotherapy, TRT is most commonly prescribed based on body surface area/weight (BSA/BW) (Lewington 2005, Zevalin 2013, Witzig 2006, Brans *et al* 2007, Buckley *et al* 2009, Lassmann *et al* 2010) or even fixed injection activities (Hoefnagel *et al* 1988, Brans *et al* 2007). However, many studies have shown that the injection activity does not correlate well with the absorbed dose. O'Connell *et al* (1993) showed that the absorbed dose to the tumor could vary by as much as three orders of magnitude for a fixed administration activity because the patient-specific pharmacokinetics were not considered. Additionally, it has been shown that there is no known association correlating a patient's BSA with tumor volume or radiation sensitivity (Kennedy *et al* 2011). Therefore, the semi-empirical nature of BSA/BW approaches could have serious clinical implications (Lam *et al* 2014) which supports a more personalized approach to prescribing TRT. In fact, a recent literature review found that only 48 out of 79 (61%) published clinical investigations established a dose-response correlation in patients undergoing TRT (Strigari *et al* 2014). Some studies that showed weak or no correlation between dose and tumor response were mostly attributed to small sample sizes and the absence of accurate and consistent dosimetry methods. Thus, dosimetry-based personalized TRT is an important clinical strategy for reducing normal tissue toxicity and optimizing tumor response.

Dosimetry-based personalized TRT prescriptions require both sophisticated radiation transport computation and medical imaging technology. There is a consensus that advanced internal dosimetry methods such as dose kernel convolution (Giap *et al* 1995, Furhang *et al* 1996, Sanchez-Garcia *et al* 2014) and Monte Carlo radiation transport (Chiavassa *et al* 2005, Hobbs *et al* 2009, Kennedy *et al* 2011, Petitguillaume *et al* 2014) voxel-level dose calculations based on patient-specific PET/CT or SPECT/CT images have the potential to be the most accurate for calculating personalized prescriptions (Stabin 2008, Lyra *et al* 2011). Like in other forms of radiation therapy, personalized TRT prescriptions rely on the ability to accurately define the tumor volume. Historically, anatomical images from CT and MR have been used to manually segment tumor volumes. However, it is well known that inter-observer variability in ROI contouring introduces one of the largest sources of imprecision in radiation therapy (Fiorino *et al* 1998, Geets *et al* 2005, Riegel *et al* 2006). This type of variability could potentially have a significant impact on TRT given the dose distributions involved in these treatments. Variability in the tumor volume could lead to uncertainties in the interpretation of the estimated tumor dose, inconsistencies in the prescription of therapeutic administration activities, and variability in the actual therapeutic dose delivered to the tumor and normal tissues. These uncertainties could lead to challenges in establishing dose-response and dose-toxicity relationships, resulting in suboptimal tumor dosing and decreased treatment efficacy, as well as unexpected toxicities to normal tissues.

To reduce this variability, several automatic or semiautomatic segmentation methods have been developed. MRI segmentation techniques include threshold-based and region-based methods, classification and clustering methods (e.g. Fuzzy c-means (FCM), Markov random fields (MRF), support vector machines (SVM), and atlas-based), and parametric and geometric deformable model methods (Liu *et al* 2014). PET and SPECT segmentation techniques include thresholding, edge detection, region growing, clustering, stochastic models, deformable models, and classifiers (Zaidi and El Naqa 2010). Threshold-based segmentation is the most commonly used method for clinical PET imaging (Zaidi and El Naqa 2010). The use of semi-quantitative values such as standard uptake values (SUVs), tumor-to-background ratios (TBRs), or maximum activities for tumor segmentation have been thoroughly investigated for ^{18}F-FDG-PET (Erdi *et al* 1997, Nestle *et al* 1999, 2005, Mah *et al* 2002, Black *et al* 2004, Biehl *et al* 2006, Drever *et al* 2007, Jentzen *et al* 2007, Boellaard *et al* 2015). Although a fixed threshold of the maximum tumor activity concentration is one of the more common methods for PET/SPECT, no single method has yet gained wide acceptance (Mawlawi and Townsend 2009). Thus, without standard protocols for multimodality tumor volume segmentation in TRT, variability in automatic segmentation methods will lead to uncertainties in patient-specific dosimetry.

The aim of this work was to investigate the magnitude of dosimetric uncertainties in patient-specific dosimetry that can arise from different automatic tumor segmentation methods.

2. Materials and methods

2.1. Image acquisition and patient data

A summary of the disease, world health organization (WHO) grade, and ^{124}I-CLR1404 injection activities are is listed in table 1 for five patients with primary or metastatic brain tumors. MR and serial PET/CT images were acquired for each patient according to the following imaging protocol. First, MR images were acquired on a GE Signa HDxt 3T clinical MRI scanner. T1 Gadolinium-enhanced axial Bravo (BRAin VOlume imaging) MR scans were acquired with a 4.2 ms echo time (TE), 10.2 ms repetition time (TR), 13° flip angle,

Table 1. Overview of the patient disease and ^{124}I-CLR1404 injection activities.

Patient	Disease	WHO grade	^{124}I-CLR1404 A_{inj} (MBq)
1	GBM	IV	182.4
2	Anaplastic astrocytoma	III	182.3
3	Metastatic melanoma	N/A	157.1
4	Astrocytoma	IV	70.3
5	Anaplastic astrocytoma	III	64.8

reconstructed image matrix size of 512 × 512, pixel size of 0.58 × 0.58 mm, and a slice thickness of 3.27 mm. PET/CT images were then acquired on a GE Discovery at 6, 24, and 48 h post intravenous infusion of approximately 64–182 MBq of ^{124}I-CLR1404 based on body surface area. CLR1404 can be radio-labeled with ^{124}I for PET imaging or ^{131}I for therapy and SPECT imaging. Clinical trials investigating efficacy of the 'diapeutic/theranostic' TRT agent CLR1404 (18-(p-iodophenyl)octadecyl phosphocholine) (Cellectar Biosciences Inc, Madison Wisconsin) are currently underway at our institution (Pinchuk *et al* 2006, Grudzinski *et al* 2014, Weichert *et al* 2014). The PET images were reconstructed using ordered subset expectation maximization (OSEM) method. The PET matrix size was 128 × 128 with a pixel size of 5.47 × 5.47 mm and a slice thickness of 3.27 mm. CT images were acquired with a tube voltage and current of 140 kVp and 8 mAs, reconstructed using the standard body kernel convolution, and used for PET image attenuation correction, scatter correction, and anatomical registration. The CT matrix size was 512 × 512 with a pixel size of 1.1045 × 1.1045 mm and a slice thickness of 3.27 mm.

Prior to segmentation, the images were coregistered and resampled to the same voxel coordinate system. Normalized mutual information affine registration was used throughout in order to account for differences in neck flexion or setup positioning that may have caused differences in the patient orientation between the MR scan and each subsequent PET/CT scan. First, the PET images were fused to the CT images at each time point. The CT images at each time point were then coregistered to the T1 MR image. The transformation of the CT images was then replicated for the corresponding PET images at each time point. Finally, the CT and PET images were resampled to match the voxel size of the MR images using a Mitchell filter kernel which offers a good compromise between ringing and blurring artifacts for both up-sampling and down-sampling (Boiangiu and Dvornic 2008).

2.2. Tumor volume segmentation

2.2.1. Single modality tumor segmentation. Both the MR and the PET images were used to segment tumor volumes using different thresholding techniques. CT images were not used for tumor segmentation because they do not provide sufficient soft tissue contrast within the brain. The optimal (i.e. ground truth) threshold level that results in the most accurate and robust segmentation of the tumor volume must be established for the specific image modality, radiopharmaceutical, tumor type, and tumor grade. These optimal thresholds have not yet been established for ^{124}I-CLR1404 PET and Gadolinium-enhanced T1 MRI for each of the specific tumor types and grades. Thus, the threshold levels used in this investigation were chosen by the physician so that the contours represented clinically realistic and reasonable tumor volumes for each patient.

The tumor was first segmented based on a Gadolinium-enhanced T1 MRI threshold. Due to variability in the level of Gadolinium-enhancement in the MR images, there was not a single threshold level that was appropriate for all of tumors. Instead, a semi-quantitative method was

employed where the threshold level for each patient was chosen based on physician guidance. The MRI threshold values of approximately 1800, 6800, 3800, 3000, and 6800 were used for patients 1–5, respectively.

PET-based enhancement metrics such as standardized uptake values (SUVs) (Huang 2000) and TBRs (Lowe *et al* 1994, Avril *et al* 1997, Higashi *et al* 1998) were also used for tumor segmentation. The SUV and TBR values were calculated based on the ^{124}I-CLR1404 PET image acquired 48 h post injection approximately corresponding to the time of peak tumor uptake. The average contralateral normal tissue SUV was calculated from a region on the contralateral side of the brain similar in size and anatomical location to the tumor. The tumor volumes were segmented using two SUV threshold levels (1.0 and 1.2) and two TBR threshold levels (1.6 and 2.0). While the optimal threshold level is radiopharmaceutical-specific, these threshold levels were chosen to be similar in magnitude to the SUV and TBR segmentation thresholds already established for other brain tumor imaging agents such as ^{18}F-FDG, ^{18}F-DOPA, ^{18}F-FET, and ^{11}C-MET (Kracht *et al* 2004, Chen *et al* 2006, Chen 2007). The same two threshold levels were able to be utilized for all of the patients due to the consistency in the CLR1404 uptake.

No hole-filling or smoothing techniques were applied to either the MR- or PET-based contours.

2.2.2. Multimodal tumor segmentation. Multi-modality imaging is often used in radiation therapy to combine the anatomical information provided by CT and MR imaging with the physiological information provided by functional PET/SPECT imaging (Bradley *et al* 2004, Ng *et al* 2005, Schwartz *et al* 2005). In order to utilize both the MRI and ^{124}I-CLR1404 PET, the impact of semi-automatic multimodal tumor segmentation was also investigated by combining the MRI and PET contours in either a union (MRI $\cup$ PET), which included all regions of MRI and PET enhancement, or an intersection (MRI $\cap$ PET), which included only regions of concordant MRI and PET enhancement. *P*-values were calculated using a two-sample Student's *t*-test to assess the statistical significance of the differences between the tumor volumes calculated for each segmentation method.

2.3. Similarity and overlap of the MRI- and PET-based tumor volumes

The similarity and overlap of the MRI- and PET-based tumor volumes were evaluated using the dice similarity coefficient (DSC), jaccard similarity coefficient (JSC), and overlap volume (OV). The DSC (Dice 1945) is defined as

$$\mathrm{DSC}\left(V_{\mathrm{MRI}}, V_{\mathrm{PET}}\right) = \frac{2\left(V_{\mathrm{MRI}} \cap V_{\mathrm{PET}}\right)}{V_{\mathrm{MRI}} + V_{\mathrm{PET}}}. \tag{1}$$

where V_{MRI} and V_{PET} are the MRI- and PET-based volumes, respectively (Jaccard 1912). The JSC is the ratio of the MRI and PET intersection and the union,

$$\mathrm{JSC}\left(V_{\mathrm{MRI}}, V_{\mathrm{PET}}\right) = \frac{V_{\mathrm{MRI}} \cap V_{\mathrm{PET}}}{V_{\mathrm{MRI}} \cup V_{\mathrm{PET}}}. \tag{2}$$

The OV is the ratio of the number of voxels in the intersection and the smallest volume,

$$\mathrm{OV}\left(V_{\mathrm{MRI}}, V_{\mathrm{PET}}\right) = \frac{V_{\mathrm{MRI}} \cap V_{\mathrm{PET}}}{\min(V_{\mathrm{MRI}}, V_{\mathrm{PET}})}. \tag{3}$$

The values for each metric range between 0 and 1. The DSC and JSC are similarity metrics and a value of 1 indicates perfect agreement between the two volumes. The OV is an overlap metric and a value of 1 indicates that the one volume is completely contained within the other.

2.4. Patient-specific TRT dosimetry

To assess the impact of the tumor segmentation methods on therapeutic dosimetry, the absorbed dose from a theoretical ^{131}I-CLR1404 therapeutic treatment was calculated from the ^{124}I-CLR1404 PET images by assuming equivalent pharmacokinetics for the two radiolabeled agents and correcting for the difference in the physical decay rates of the radionuclides (Sgouros *et al* 2004). Voxelized patient-specific absorbed dose distributions from ^{131}I-CLR1404 were calculated using the RAPID platform. RAPID is a patient-specific Monte Carlo 3D internal dosimetry platform that has been described in previous publications (Besemer *et al* 2013, 2015, Besemer and Bednarz 2014). Within the platform, the CT and PET images were used to define the geometry and radionuclide source distribution, respectively. The ^{131}I-CLR1404 absorbed dose rate at each time point was calculated with the Monte Carlo code Geant4 (Agnostinelli 2003). The absorbed dose distribution was calculated by time-integrating the dose rate on a voxel-by-voxel basis using a piecewise linear fit with the uptake linearly extrapolated back from the first two time points and the decay after the last time point fit extrapolated using an exponential physical decay. Because it is assumed that the absorbed dose scales linearly with injection activity, the absorbed dose was normalized by the injection activity and calculated in units of Gy GBq^{-1} of ^{131}I-CLR1404 injected. Patient-specific 3D voxel-level dose distributions, DVHs, and mean tumor doses were generated. The squared Pearson correlation coefficient (R^2) and p-values were calculated to quantify the linear correlation between the tumor volume and mean tumor dose for each patient.

3. Results

3.1. Tumor volumes

The tumor volumes are shown in figure 1 for each threshold segmentation method. For most patients, the CLR1404 uptake extended beyond the region of MRI enhancement and resulted in larger PET-based tumor volumes. TBR volumes were generally larger than the SUV volumes. The TBR, SUV, and MRI tumor volumes ranged from 2.3–63.9 cc, 0.1–34.7 cc, and 0.4–11.8 cc, respectively. The SUV 1.0 tumor volumes were 15–74% larger than the SUV 1.2 and the TBR 1.6 tumor volumes were 7–35% larger than the TBR 2.0. Because smaller MRI contours were usually contained within larger PET contours, the MRI $\cup$ PET contours were generally similar in size to the larger PET-based contour volumes and the MRI $\cap$ PET contours were similar to the smaller MRI-based contour volumes. The p-values assessing the statistical significance of the differences in the tumor volume for each combination of tumor segmentation method are shown in table 2. Overall, 52 (67%) of the tumor volume comparisons were not statistically significant, 12 (15%) were moderately significant ($0.01 \leqslant p < 0.05$) and 14 (18%) were strongly significant with ($p < 0.01$). Notably, the TBR and MRI $\cup$ TBR tumor volumes (for both the 1.6 and 2.0 threshold levels) were significantly different from the majority of the other tumor volumes.

3.2. MRI and PET similarity and overlap metrics

The DSC, JSC, and OV metrics for each MRI and PET combination are shown in table 3. The average $\pm$ stdev (range) was 0.30 ± 0.17 (0.02–0.67), 0.19 ± 0.13 (0.01–0.51), and 0.75 ± 0.29 (0.05–1.00) for the DSC, JSC, and OV, respectively. Overall, the DSC and JSC values were small for both the MRI-SUV and MRI-TBR combinations because the regions of PET uptake were generally larger than the regions of MRI enhancement. The SUV volumes

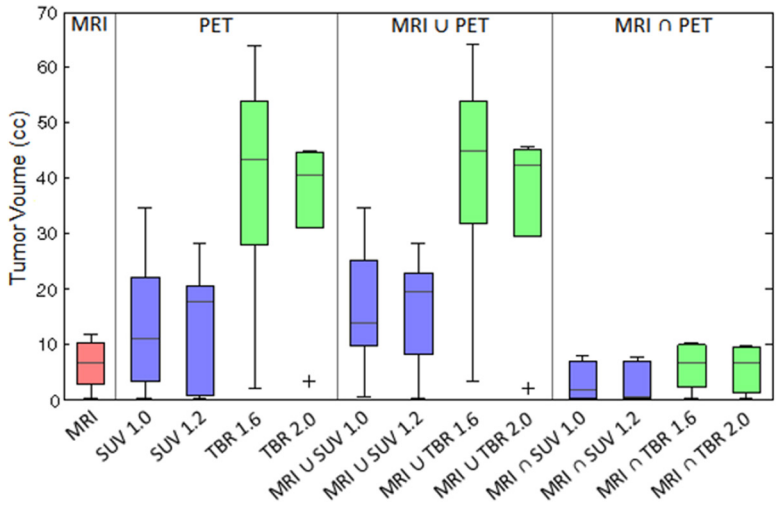

Figure 1. Box plot comparing the tumor contour volumes for each threshold segmentation method. In general, the TBR tumor volumes were larger (2.3–63.9 cc) than the SUV (0.1–34.7 cc) and MRI (0.4–11.8 cc) volumes. Because the smaller MRI contours were usually contained within the larger PET (SUV and TBR) contours, the MRI ∪ PET union volumes were generally similar to the PET-threshold contour volumes and the MRI ∩ PET intersection volumes were similar to the MRI-threshold contour volumes.

were similar in size to the MRI volumes so the MRI-SUV had slightly larger DSC and JSC values compared to the MRI-TBR. Regions of MRI enhancement were usually contained within the regions of CLR1404 PET uptake, which resulted in large OV values for the MRI-SUV and MRI-TBR combinations. For Patient 2, the MRI volume was completely contained within all SUV and TBR volumes so the all the OV values were unity.

3.3. Dosimetry

3.3.1. Single modality tumor segmentation. The MRI, ^{124}I-CLR1404 PET, and ^{131}I-CLR1404 dose distributions for each patient are shown in figure 2. The individual MRI, SUV, and TBR threshold-based tumor contours are overlaid on the MRI image and the resulting DVHs are also shown. Significant differences in the shape of the MRI, SUV, and TBR tumor DVHs were observed for each patient. Patient 2 demonstrated CLR1404 uptake extending beyond the MRI enhancement resulting in a larger dose in the MRI tumor volume. Patient 4 had notably high discordance between the MRI enhancement and the ^{124}I-CLR1404 avid areas, which resulted in a smaller dose in the MRI tumor volume compared to the SUV and TBR volumes. For the other three patients, the dose within the MRI tumor volume was generally larger than the dose within the TBR volumes and smaller than the dose within SUV volumes.

The SUV mean doses ranged from 0.64–1.37 Gy GBq^{-1} and were generally higher than the TBR mean doses which ranged from 0.48–0.99 Gy GBq^{-1}. The MRI mean doses ranged from 0.50–1.67 Gy GBq^{-1}. The larger SUV 1.0 volumes resulted in 7–15% smaller mean doses compared for the SUV 1.2 volumes and the larger TBR 1.6 volumes resulted in 6–12% smaller mean doses compared to the TBR 2.0.

Table 2. The p-values assessing the statistical significance of the difference in the tumor volume between each contour combination. Overall, 14 (18%) were strongly significant with $p < 0.01$ (indicated by [a]), 12 (15%) were moderately significant with $0.01\ p < 0.05$ (indicated by [b]), and 52 (67%) of the tumor volume comparisons were not statistically significant.

	Tumor volume difference p-value											
Tumor Contour	SUV 1.0	MRI ∪ SUV 1.0	MRI ∩ SUV 1.0	SUV 1.2	MRI ∪ SUV 1.2	MRI ∩ SUV 1.2	TBR 1.6	MRI ∪ TBR1.6	MRI ∩ TBR 1.6	TBR 2.0	MRI ∪ TBR 2.0	MRI ∩ TBR 2.0
MRI	0.306	0.128	0.265	0.330	0.109	0.230	0.011[b]	0.011[b]	0.856	0.011[b]	0.011[b]	0.739
SUV 1.0	—	0.708	0.143	0.899	0.761	0.134	0.052	0.050[b]	0.270	0.081	0.073	0.245
MRI ∪ SUV 1.0	—	—	0.052	0.597	0.918	0.048[b]	0.075	0.072	0.109	0.123	0.110	0.097
MRI ∩ SUV 1.0	—	—	—	0.140	0.037[b]	0.909	0.007[a]	0.006[a]	0.323	0.006[a]	0.006[a]	0.414
SUV 1.2	—	—	—	—	0.640	0.130	0.040[b]	0.038[b]	0.287	0.059	0.054	0.257
MRI ∪ SUV 1.2	—	—	—	—	—	0.034[b]	0.061	0.057	0.090	0.095	0.085	0.079
MRI ∩ SUV 1.2	—	—	—	—	—	—	0.006[a]	0.006[a]	0.280	0.006[a]	0.006[a]	0.362
TBR 1.6	—	—	—	—	—	—	—	0.971	0.010[b]	0.620	0.675	0.009[a]
MRI ∪ TBR 1.6	—	—	—	—	—	—	—	—	0.010[a]	0.594	0.649	0.009[a]
MRI ∩ TBR 1.6	—	—	—	—	—	—	—	—	—	0.010[b]	0.009[a]	0.871
TBR 2.0	—	—	—	—	—	—	—	—	—	—	0.933	0.009[a]
MRI ∪ TBR 2.0	—	—	—	—	—	—	—	—	—	—	—	0.009[a]

Table 3. The DSC, JSC, and OV similarity and overlap metrics for each patient for the MRI and each PET combination. The average (ave) and standard deviation (stdev) over all five patients is also shown.

	DSC				JSC				OV			
Patient	SUV 1.0	SUV 1.2	TBR 1.6	TBR 2.0	SUV 1.0	SUV 1.2	TBR 1.6	TBR 2.0	SUV 1.0	SUV 1.2	TBR 1.6	TBR 2.0
1	0.27	0.11	0.27	0.34	0.15	0.06	0.16	0.21	0.44	0.55	0.96	0.91
2	0.33	0.39	0.24	0.26	0.20	0.24	0.14	0.15	1.00	1.00	1.00	1.00
3	0.67	0.45	0.22	0.32	0.51	0.29	0.12	0.19	0.71	0.98	1.00	0.98
4	0.02	0.09	0.14	0.08	0.01	0.03	0.08	0.04	0.05	0.16	0.82	0.45
5	0.53	0.57	0.37	0.38	0.36	0.39	0.23	0.23	0.68	0.65	0.87	0.84
Ave	0.36	0.32	0.25	0.28	0.25	0.20	0.14	0.17	0.58	0.67	0.93	0.84
Stdev	0.25	0.21	0.08	0.12	0.19	0.16	0.06	0.07	0.35	0.34	0.08	0.23

3.3.2. Multimodal tumor segmentation. The DVHs of the union and intersection combination contours for the TBR and SUV thresholds are shown in figure 3 for Patient 1. These are representative of the results seen in the other patients (data not shown). In general, the union contours were similar in size to the PET-based contour volumes so the union contour DVHs were similar in shape to the SUV/TBR DVHs. Conversely, the intersection contours were similar to the MRI-based contour volumes so the intersection contour DVHs were similar in shape to the MRI DVHs.

The spread in mean tumor doses for each tumor segmentation method is shown in figure 4 for each patient. The mean ^{131}I-CLR1404 tumor doses ranged from 0.48 to 1.75 Gy GBq^{-1}, with a standard deviation between 0.07 and 0.37 Gy GBq^{-1}, and a coefficient of variation of 11–28%. The ratio of maximum to minimum mean doses for each patient ranged from 1.4 to 2.0.

The correlation between the mean tumor dose and the tumor volume calculated for each contouring method is shown in figure 5. The relationship was very linear for Patient 2 ($R^2 = 0.98$, $p < 0.001$), Patient 3 ($R^2 = 0.91$, $p < 0.001$), and Patient 5 ($R^2 = 0.94$, $p < 0.001$). For these patients, the different tumor volumes were relatively concentric so the average dose decreased as the volume increased to include more low dose regions. For Patient 1 ($R^2 = 0.30$, $p = 0.34$) and Patient 4 ($R^2 = 0.09$, $p = 0.78$), the mean dose also generally decreased with increasing volumes but the relationship was not significantly linear. The tumor volumes for these two patients were relatively less concentric and there were larger discordant regions of MR and PET enhancement.

4. Discussion

Patient-specific dose calculations rely on accurate tumor delineation in order to best estimate the therapeutic dose from pre-treatment images. Because the definition of the target volume can be a potential source of uncertainty in TRT, automatic tumor segmentation methods have been applied with the intention of reducing inter-observer contouring variability. However, the results of this work demonstrate that the tumor volume and tumor dose from ^{131}I-CLR1404 are highly sensitive to the imaging modality (e.g. PET or MRI), PET enhancement metric (e.g. SUV or TBR), and threshold level used for tumor volume segmentation.

The MRI enhancement regions were generally contained within the larger regions of CLR1404 PET enhancement, ultimately contributing to relatively large OV values and regions of MRI+/PET+ concordance. However, the low DSC and JSC similarity values indicate that

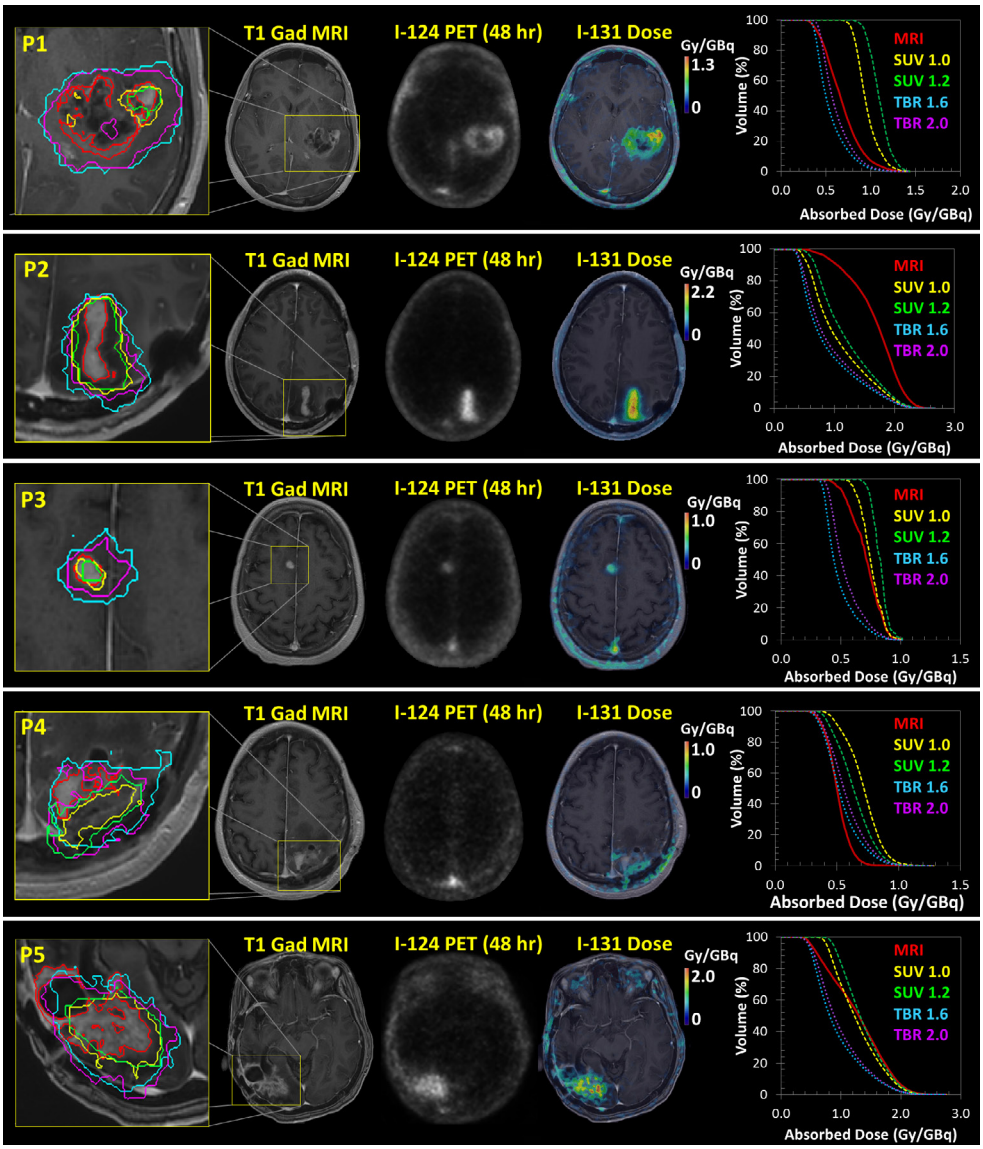

Figure 2. The MRI, 48 hr post injection ^{124}I-CLR1404 PET, and ^{131}I-CLR1404 dose distributions for each patient. The MRI, SUV, and TBR threshold-based tumor contours and the resulting DVHs are also shown.

there were significant differences in size between the MRI and PET based contours that resulted in discordant MRI−/PET+ regions, and to a lesser extent, discordant MRI+/PET- regions. For Patient 2, the CLR1404 uptake extended beyond the MRI enhancement, resulting in a larger dose in the MRI tumor volume and intersection tumor volumes. Patient 4 exhibited the largest discordance between the MRI enhancement and the ^{124}I-CLR1404 avid areas resulting in a smaller dose in the MRI tumor volume and intersection tumor volumes. Interestingly, Patient 2 had the largest dosimetric variation between the different contouring methods, which is surprising because the high levels of CLR1404 uptake and MRI enhancement, with large

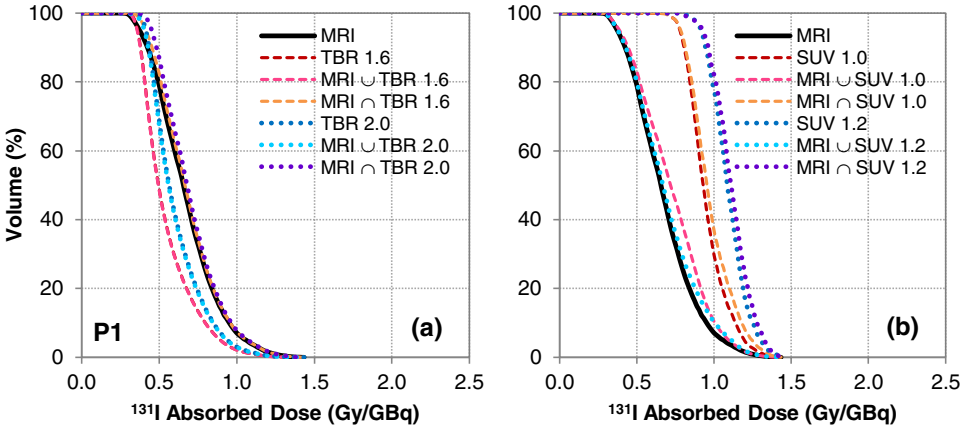

Figure 3. DVHs of the union and intersection combination contours for the (a) TBR and (b) SUV thresholds for patient 1. These are representative of the results seen in the rest of the patients where the doses within the TBR contours were typically smaller than the MRI contours because the TBR contours were larger in size and vice versa for the SUV contours. Additionally, the union contours were generally similar in size to the PET-based contour volumes so the DVHs based on the union contours were similar to the SUV/TBR DVHs. Conversely, the intersection contours were similar to the MRI-based contour volumes so the DVHs based the intersection contours were similar to the MRI DVHs.

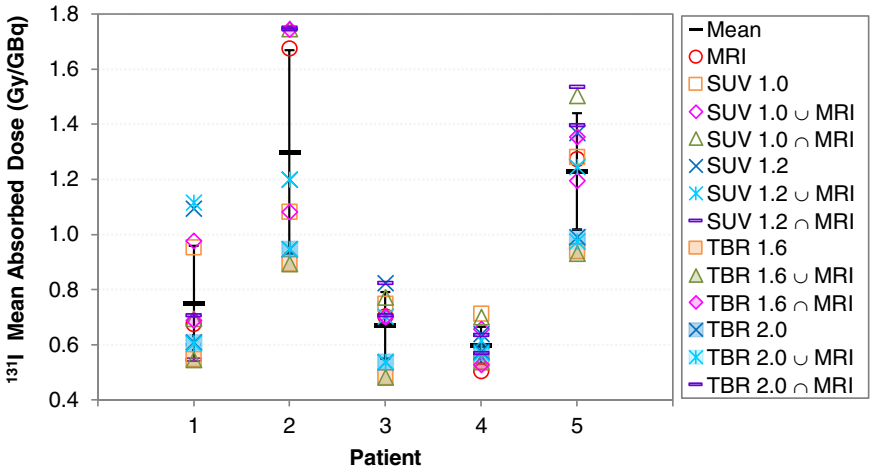

Figure 4. Mean tumor doses for each patient. The error bars represent the standard deviation. Note that the larger TBR contours (filled markers) generally had smaller mean doses and the smaller SUV contours (unfilled markers) generally had larger mean doses.

concordant MRI+/PET+ regions, represent the near ideal case for multi-modality tumor segmentation. However, the MRI−/PET+ discordant regions were the main source of the large difference between the doses in the MRI- and PET-based tumor volumes. Also, surprising was the fact that Patient 4, which had relatively low levels of CLR1404 uptake and both MRI−/PET+ and MRI+/PET− discordant regions (especially for the SUV), resulted in the smallest

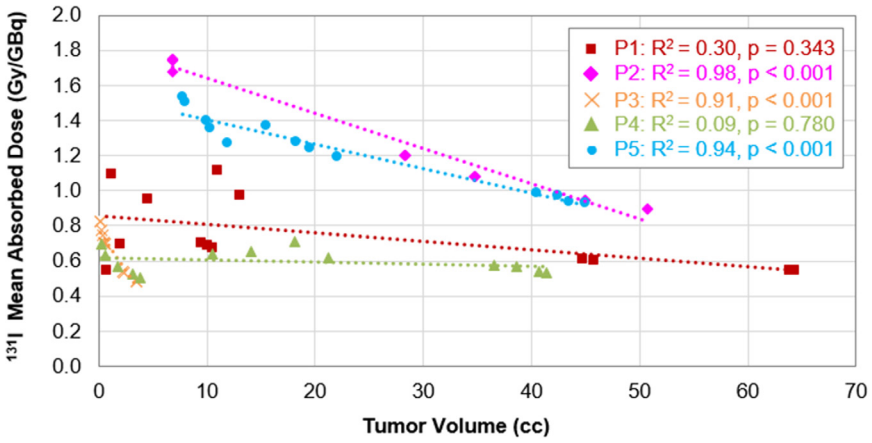

Figure 5. Correlation between the mean tumor dose and the tumor contour volumes for each patient. The Pearson correlation coefficient (R^2) and p-values of the linear correlation are also shown.

variation in the mean tumor doses between the different contouring methods. Patient 4 had the smallest relative MRI+/PET+ concordant regions. For this case, it seems that because the CLR1404 uptake was relatively low, the MRI−/PET+ regions only contained slightly more CLR1404 uptake and dose resulting in smaller variations in the tumor doses.

The two different PET enhancement metrics, TBR and SUV, had different impacts on both tumor volume and dose, as did their respective threshold levels. In each case, the TBR volumes were larger than the SUV volumes. Since the size of the SUV volumes were similar to the MRI volumes, the MRI-SUV combinations had slightly larger DSC and JSC similarity values compared to the MRI-TBR combinations. The TBR contours resulted in smaller tumor doses because of dose averaging over a larger volume. As expected, the use of lower threshold levels resulted in larger tumor volumes and smaller tumor doses for both enhancement metrics.

Some of the contouring methods resulted in significant differences in the shape of the tumor DVHs. The most notable difference occurred in Patient 2 where the MRI contour indicated significantly more dose homogeneity within the tumor compared to both the SUV and TBR contours. Conversely, the MRI contour for Patient 5 indicated slightly less dose homogeneity than the PET-based contours because the MRI DVH had a larger low dose shoulder. Accurate qualification of the tumor dose homogeneity is important because non-uniform dose distributions in TRT can have significant clinical implications for the treatment response and toxicity (O'Donoghue 1999, Amro *et al* 2010, Hanaoka *et al* 2014, Hrycushko *et al* 2011). Specifically, one study by Hrycushko *et al* (2011), investigating the impact of ^{186}Re-liposome dose heterogeneity in head and neck squamous cell carcinoma mouse xenografts, found that cold spots resulted in reduced tumor control (i.e. tumor shrinkage) analogous to the results seen for human patients undergoing external beam radiotherapy (Niemierko and Goitein 1991, Tomé and Fowler 2002). While the magnitude of the clinical implications is likely specific to the treatment modality, radiopharmaceutical, and tumor type, it is reasonable to conclude that the differences in tumor dose heterogeneity due to variations in tumor segmentation methods found in this study would likely have an impact on the therapeutic outcome.

For all patients, the mean dose decreased as the tumor volume increased due to the inclusion of more low dose regions within the larger contour. The relationship was significantly linear for the Patients 2, 3 and 5 which had fairly concentric tumor volumes (i.e. large MRI-PET

OV values). For the other two patients, the mean dose only slightly decreased with increasing tumor volume, likely due to the necrotic tissue in the middle of tumor for Patient 1 and the large discordance between the MRI enhancement and the ^{124}I-CLR1404 avid areas for Patient 4. The coefficient of variation of the mean tumor doses over all target volumes for each patient ranged from 11–28% whereas the ratio of the maximum to minimum mean tumor doses ranged from 1.4 to 2.0. Thus, depending on the tumor segmentation method used, the estimated mean tumor dose could deviate by up to 200% which could lead to higher normal tissue toxicities and/or reduced treatment efficacy. Because this pilot study only utilized five illustrative brain cancer patients imaged with ^{124}I-CLR1404 PET, the magnitude of dosimetric variations may be different for patients imaged with other molecular agents and for patients with different tumor histologies, grades, or anatomic locations. Additionally, the dosimetric sensitivity to tumor volume differences may depend on the patient-specific tumor microenvironment. Thus, future work will investigate the correlation between each of these factors and the dosimetric variation caused by the use of multi-modality tumor volume segmentation methods with a larger sample size of patients.

While this work highlights the sensitivity of TRT dosimetry to the employed tumor segmentation methods for a particular molecular agent, it is not possible to speculate which enhancement metric or threshold level is the most accurate. This is planned as an important aim of a future clinical study. Ultimately, each contouring method needs to be evaluated within the framework of its sensitivity and specificity for each agent, tumor type, and imaging modality, and verified with the histopathological characterization of tissue biopsies and actual clinical outcomes as the ground truth.

The fact that the optimal threshold level has to be determined for each specific application is one of the major limitations of threshold-based contouring. This is especially cumbersome for PET imaging since the optimal level must be determined for the specific radiopharmaceutical and enhancement metric (e.g. SUV, TBR, maximum activity). One promising alternative is gradient edge detection which has been shown to be both accurate and robust for a variety of applications (Geets *et al* 2007, Werner-Wasik *et al* 2012). One of the major drawbacks specific to the threshold-based MR contouring method is that it is only semi-automated since the threshold level must be uniquely chosen for each individual patient based on physician guidance. While all the MR images in this study were obtained using the same scanner, field strength, imaging sequence, and contrast agent, variability in the MR signal intensity can still be dependent on the specific tumor type and grade and be caused by physiological motion, time-variant system performance (e.g. due to drift of scanners over time), and imaging gradient non-linearity (Zhu *et al* 2011, Mirzaalian *et al* 2015). Scanner harmonization methods have been proposed to produce more consistent MR signals across different institutions, scanners, and body sites (Mirzaalian *et al* 2015). Such normalization of the MR signal will have to be implemented before any standard protocols for MR threshold-based contouring can be practically utilized.

While the goal of this work was not to suggest an optimal threshold-based contouring method for brain tumors in TRT, it is clear that a multi-modality imaging approach, utilizing the different information provided by of both MR and PET, would be ideal. MR gadolinium enhancement is a sensitive indicator of blood-brain barrier breakdown. However, malignant gliomas can sometimes infiltrate brain tissue without disrupting the blood-brain barrier and large parts of low grade gliomas may be non-enhancing (Wen *et al* 2010). Additionally, gadolinium enhancement can also be affected by inflammation, seizure activity, postsurgical changes, necrosis, ischemia, antiangiogenic agents, corticosteroids, and differences in radiographic imaging techniques (Wen *et al* 2010). Functional imaging modalities, such as PET and

SPECT, can measure physiological characteristics of cancer cells such as changes in metabolism, blood flow, chemical composition, and absorption. PET imaging has shown improved sensitivity and specificity, compared to CT and MR, for tumor cell localization, detection of lymph node involvement, and staging (Dwamena *et al* 1999, Weber *et al* 1999, Boiselle 2000, Pieterman *et al* 2000). Specifically, CLR1404 is a phospholipid ether analog that is taken up with high sensitivity and specificity in the lipid rafts which are overexpressed in cancer cells (Weichert *et al* 2014). The disadvantages of PET and SPECT imaging include lower spatial resolution, higher cost, and increased imaging dose from the radioisotope. Thus, a multimodality imaging approach could draw upon the strengths of each modality and allows for the tumor to be segmented based on both anatomical and functional information.

The large range of dosimetric uncertainties reported in this study underscore the need for standard protocols for tumor segmentation in TRT dosimetry. The medical internal radiation dose (MIRD) Committee of the SNMMI is one of the primary resources for the standardization of internal dosimetry practices. The MIRD Pamphlet No. 23 (Dewaraja *et al* 2012), provides guidance on quantitative SPECT imaging for 3D internal dosimetry, but only briefly discussed recommendations for target definition with SPECT imaging. It states that the preferred method is to define the target using manual or automatic threshold-based contouring based on high-resolution anatomic images (such as a CT) and propagate those contours to the SPECT images. For SPECT-based target delineation, either a fixed threshold or more sophisticated adaptive thresholding methods are recommended. Despite the acknowledgement that high resolution PET imaging is emerging as an important modality for the delineation of target volumes, no recommendations were given for PET-based target delineation. To the best of our knowledge no other specific guidance on tumor segmentation for TRT has been published. We anticipate that this work will highlight the importance of characterizing and standardizing tumor segmentation methods in TRT.

5. Conclusion

The goal of this study was to investigate the impact of PET and MRI threshold-based tumor segmentation on TRT dosimetry in patients with primary and metastatic brain tumors. Significant differences in the shape of the MRI, SUV, and TBR tumor dose volume histograms (DVHs) were observed for each patient. Depending on the thresholding method, deviations in the ^{131}I-CLR1404 mean tumor doses up to a factor of two were observed. Uncertainties in the tumor dose of this magnitude could lead to challenges establishing dose-response and dose-toxicity relationships, suboptimal tumor doses and loss of treatment efficacy, as well as unexpected normal tissue toxicities. Thus, the results of this investigation clearly demonstrate the need for standard protocols for multimodality tumor volume segmentation in TRT dosimetry.

Acknowledgments

The authors would like to thank the UW Center for High Throughput Computing (CHTC) for the use of their cluster and their computational support. JPW is a founder of Cellectar Biosciences, Inc., which owns the licensing rights to CLR1404 and related technologies. JSK is partially supported by the Roger Loff Memorial Fund for GBM Research. The authors have no relevant conflicts of interest to disclose. This study was partially funded by UL1TR000427, P30CA014520, and R01CA158800.

References

Agnostinelli S 2003 Geant4—a simulation toolkit *Nucl. Instrum. Methods Phys. Res.* A **506** 250–303

Amro H, Wilderman S J, Dewaraja Y K and Roberson P L 2010 Methodology to incorporate biologically effective dose and equivalent uniform dose in patient-specific 3-dimensional dosimetry for non-Hodgkin lymphoma patients targeted with 131I-tositumomab therapy *J. Nucl. Med.* **51** 654–9

Avril N, Bense S, Ziegler S I and Dose J 1997 Breast imaging with fluorine-18-FDG PET: quantitative image analysis *J. Nucl. Med.* **38** 1186

Besemer A and Bednarz B 2014 SU-ET-345: validation of a patient-specific Monte Carlo targeted radionuclide therapy dosimetry platform *Med. Phys.* **41** 303–4

Besemer A, Grudzinski J, Titz B and Bednarz J 2015 WE-EF-BRA-04: evaluation of dosimetric uncertainties in individualized targeted radionuclide therapy (TRT) treatment planning using pre-clinical data *Med. Phys.* **42** 3675–5

Besemer A, Grudzinski J, Titz B, Wickre P, Hall L, Weichert J and Bednarz B 2013 SU-F-500-01: towards personalized dosimetry using diapeutic radiopharmaceuticals *Med. Phys.* **40** 382–2

Biehl K J, Kong F-M, Dehdashti F, Jin J-Y, Mutic S, El Naqa I, Siegel B A and Bradley J D 2006 18F-FDG PET definition of gross tumor volume for radiotherapy of non–small cell lung cancer: is a single standardized uptake value threshold approach appropriate? *J. Nucl. Med.* **47** 1808–12

Black Q C, Grills I S, Kestin L L, Wong C-Y O, Wong J W, Martinez A A and Yan D 2004 Defining a radiotherapy target with positron emission tomography *Int. J. Radiat. Oncol. Biol. Phys.* **60** 1272–82

Boellaard R *et al* 2015 FDG PET and PET/CT: EANM procedure guidelines for tumour imaging: version 2.0 *Eur. J. Nucl. Med. Mol. Imaging* **42** 328–54

Boiangiu C-A and Dvornic A I 2008 Methods of bitonal image conversion for modern and classic documents *WSEAS Trans. Comput.* **7** 1081–90

Boiselle P 2000 MR imaging of thoracic lymph nodes. A comparison of computed tomography and positron emission tomography *Magn. Reson. Imaging Clin. North Am.* **8** 33–41

Bradley J, Thorstad W L, Mutic S, Miller T R, Dehdashti F, Siegel B A, Bosch W and Bertrand R J 2004 Impact of FDG-PET on radiation therapy volume delineation in non-small-cell lung cancer *Int. J. Radiat. Oncol. Biol. Phys.* **59** 78–86

Brans B, Bodei L, Giammarile F, Lindén O, Luster M, Oyen W and Tennvall J 2007 Clinical radionuclide therapy dosimetry: the quest for the 'Holy Gray' *Eur. J. Nucl. Med. Mol. Imaging* **34** 772–86

Buckley S E, Chittenden S J, Saran F H, Meller S T and Flux G D 2009 Whole-body dosimetry for individualized treatment planning of 131I-MIBG radionuclide therapy for neuroblastoma *J. Nucl. Med.* **50** 1518–24

Chen W 2007 Clinical applications of PET in brain tumors *J. Nucl. Med.* **48** 1468–81

Chen W, Silverman D H, Delaloye S, Czernin J, Kamdar N, Pope W, Satyamurthy N, Schiepers C and Cloughesy T 2006 18F-FDOPA PET imaging of brain tumors: comparison study with 18F-FDG PET and evaluation of diagnostic accuracy *J. Nucl. Med.* **47** 904–11

Chiavassa S, Lemosquet A, Aubineau-Laniece I, De Carlan L, Clairand I, Ferrer L, Bardiès M, Franck D and Zankl M 2005 Dosimetric comparison of Monte Carlo codes (EGS4, MCNP, MCNPX) considering external and internal exposures of the Zubal phantom to electron and photon sources *Radiat. Prot. Dosim.* **116** 631–5

Dewaraja Y K, Frey E C, Sgouros G, Brill A B, Roberson P, Zanzonico P B and Ljungberg M 2012 MIRD pamphlet no. 23: quantitative SPECT for patient-specific 3-dimensional dosimetry in internal radionuclide therapy *J. Nucl. Med.* **53** 1310–25

Dice L R 1945 Measures of the amount of ecologic association between species *Ecology* **26** 297–302

Drever L, Roa W, Mcewan A and Robinson D 2007 Iterative threshold segmentation for PET target volume delineation *Med. Phys.* **34** 1253–65

Dwamena B A, Sonnad S S, Angobaldo J O and Wahl R L 1999 Metastases from non-small cell lung cancer: mediastinal staging in the 1990s—meta-analytic comparison of PET and CT *Radiology* **213** 530–6

Erdi Y E, Mawlawi O, Larson S M, Imbriaco M, Yeung H, Finn R and Humm J L 1997 Segmentation of lung lesion volume by adaptive positron emission tomography image thresholding *Cancer* **80** 2505–9

Fiorino C, Reni M, Bolognesi A, Cattaneo G M and Calandrino R 1998 Intra-and inter-observer variability in contouring prostate and seminal vesicles: implications for conformal treatment planning *Radiother. Oncol.* **47** 285–92

Furhang E E, Sgouros G and Chui C S 1996 Radionuclide photon dose kernels for internal emitter dosimetry *Med. Phys.* **23** 759–64

Geets X, Daisne J-F, Arcangeli S, Coche E, De Poel M, Duprez T, Nardella G and Grégoire V 2005 Inter-observer variability in the delineation of pharyngo-laryngeal tumor, parotid glands and cervical spinal cord: comparison between CT-scan and MRI *Radiother. Oncol.* **77** 25–31

Geets X, Lee J A, Bol A, Lonneux M and Grégoire V 2007 A gradient-based method for segmenting FDG-PET images: methodology and validation *Eur. J. Nucl. Med. Mol. Imaging* **34** 1427–38

Giap H B, Macey D J, Bayouth J E and Boyer A L 1995 Validation of a dose-point kernel convolution technique for internal dosimetry *Phys. Med. Biol.* **40** 365

Grudzinski J J, Titz B, Kozak K, Clarke W, Allen E, Trembath L, Stabin M, Marshall J, Cho S Y and Wong T Z 2014 A phase 1 study of 131 I-CLR1404 in patients with relapsed or refractory advanced solid tumors: dosimetry, biodistribution, pharmacokinetics, and safety *PloS One* **9** e111652

Hanaoka K, Hosono M, Tatsumi Y, Ishii K, Im S-W, Tsuchiya N, Sakaguchi K and Matsumura I 2014 Heterogeneity of intratumoral (1 1 1) In-ibritumomab tiuxetan and (18)F-FDG distribution in association with therapeutic response in radioimmunotherapy for B-cell non-Hodgkin's lymphoma *Eur. J. Nucl. Med. Mol, Imaging Res.* **5** 10

Higashi K, Nishikawa T, Seki H, Oguchi M, Nambu Y, Ueda Y, Yuasa K, Tonami H, Okimura T and Yamamoto I 1998 Comparison of fluorine-18-FDG PET and thallium-201 SPECT in evaluation of lung cancer *J. Nucl. Med.* **39** 9–14

Hobbs R F, Wahl R L, Lodge M A, Javadi M S, Cho S Y, Chien D T, Ewertz M E, Esaias C E, Ladenson P W and Sgouros G 2009 124I PET-Based 3D-RD dosimetry for a pediatric thyroid cancer patient: real-time treatment planning and methodologic comparison *J. Nucl. Med.* **50** 1844–7

Hoefnagel C, De Kraker J and Voûte P 1988 Radionuclide treatment of neuroblastoma using 131I meta-iodobenzylguanidine *Molecular Biology and Genetics of Childhood Cancers: Approaches to Neuroblastoma* (New York: Wiley)

Hrycushko B A, Ware S, Li S and Bao A 2011 Improved tumour response prediction with equivalent uniform dose in pre-clinical study using direct intratumoural infusion of liposome-encapsulated 186Re radionuclides *Phys. Med. Biol.* **56** 5721

Huang S-C 2000 Anatomy of SUV *Nucl. Med. Biol.* **27** 643–6

Jaccard P 1912 The distribution of the flora in the alpine zone *New Phytol.* **11** 37–50

Jentzen W, Freudenberg L, Eising E G, Heinze M, Brandau W and Bockisc A 2007 Segmentation of PET volumes by iterative image thresholding *J. Nucl. Med.* **48** 108–14

Kennedy A, Dezarn W and Weiss A 2011 Patient specific 3D image-based radiation dose estimates for 90Y microsphere hepatic radioembolization in metastatic tumors *J. Nucl. Med. Radiat. Ther.* **2** 1–8

Kracht L W, Miletic H, Busch S, Jacobs A H, Voges J, Hoevels M, Klein J C, Herholz K and Heiss W-D 2004 Delineation of brain tumor extent with [11C] l-methionine positron emission tomography local comparison with stereotactic histopathology *Clin. Cancer Res.* **10** 7163–70

Lam M G, Louie J D, Abdelmaksoud M H, Fisher G A, Cho-Phan C D and Sze D Y 2014 Limitations of body surface area–based activity calculation for radioembolization of hepatic metastases in colorectal cancer *J. Vascular Intervent. Radiol.* **25** 1085–93

Lassmann M, Reiners C and Luster M 2010 Dosimetry and thyroid cancer: the individual dosage of radioiodine *Endocr.-Relat. cancer* **17** R161–72

Lewington V J 2005 Bone-seeking radionuclides for therapy *J. Nucl. Med.* **46** 38S–47S

Liu J, Li M, Wang J, Wu F, Liu T and Pan Y 2014 A survey of MRI-based brain tumor segmentation methods *Tsinghua Sci. Technol.* **19** 578–95

Lowe V J, Hoffman J M, Delong D M, Patz E F and Coleman R E 1994 Semiquantitative and visual analysis of FDG-PET images in pulmonary abnormalities *J. Nucl. Med.* **35** 1771–6

Lyra M, Lagopati N, Charalambatou P and Vamvakas I 2011 Patient-specific dosimetry in radionuclide therapy *Radiat. Prot. Dosim.* **147** 258–63

Mah K, Caldwell C B, Ung Y C, Danjoux C E, Balogh J M, Ganguli S N, Ehrlich L E and Tirona R 2002 The impact of 18 FDG-PET on target and critical organs in CT-based treatment planning of patients with poorly defined non-small-cell lung carcinoma: a prospective study *Int. J. Radiat. Oncol. Biol. Phys.* **52** 339–50

Mawlawi O and Townsend D W 2009 Multimodality imaging: an update on PET/CT technology *Eur. J. Nucl. Med. Mol. Imaging* **36** 15–29

Mirzaalian H, De Pierrefeu A, Savadjiev P, Pasternak O, Bouix S, Kubicki M, Westin C-F, Shenton M E and Rathi Y 2015 Harmonizing diffusion mri data across multiple sites and scanners *Int. Conf. on Medical Image Computing and Computer-Assisted Intervention* (Berlin: Springer) pp 12–9

Nestle U, Kremp S, Schaefer-Schuler A, Sebastian-Welsch C, Hellwig D, Rübe C and Kirsch C-M 2005 Comparison of different methods for delineation of 18F-FDG PET–positive tissue for target volume definition in radiotherapy of patients with non–small cell lung cancer *J. Nucl. Med.* **46** 1342–8

Nestle U, Walter K, Schmidt S, Licht N, Nieder C, Motaref B, Hellwig D, Niewald M, Ukena D and Kirsch C M 1999 18 F-Deoxyglucose positron emission tomography (FDG-PET) for the planning of radiotherapy in lung cancer: high impact in patients with atelectasis *Int. J. Radiat. Oncol. Biol. Phys.* **44** 593–7

Ng S-H, Yen T-C, Liao C-T, Chang J T-C, Chan S-C, Ko S-F, Wang H-M and Wong H-F 2005 18F-FDG PET and CT/MRI in oral cavity squamous cell carcinoma: a prospective study of 124 patients with histologic correlation *J. Nucl. Med.* **46** 1136–43

Niemierko A and Goitein M 1991 Calculation of normal tissue complication probability and dose-volume histogram reduction schemes for tissues with a critical element architecture *Radiother. Oncol.* **20** 166–76

O'Connell M, Flower M, Hinton P, Harmer C and Mccready V 1993 Radiation dose assessment in radioiodine therapy. Dose-response relationships in differentiated thyroid carcinoma using quantitative scanning and PET *Radiother. Oncol.* **28** 16–26

O'Donoghue J A 1999 Implications of nonuniform tumor doses for radioimmunotherapy *J. Nucl. Med.* **40** 1337–41

Petitguillaume A, Bernardini M, Hadid L, De Labriolle-Vaylet C, Franck D and Desbrée A 2014 Three-dimensional personalized Monte Carlo dosimetry in 90Y resin microspheres therapy of hepatic metastases: nontumoral liver and lungs radiation protection considerations and treatment planning optimization *J. Nucl. Med.* **55** 405–13

Pieterman R M, Van Putten J W, Meuzelaar J J, Mooyaart E L, Vaalburg W, Koëter G H, Fidler V, Pruim J and Groen H J 2000 Preoperative staging of non–small-cell lung cancer with positron-emission tomography *New Engl. J. Med.* **343** 254–61

Pinchuk A N, Rampy M A, Longino M A, Scott Skinner R W, Gross M D, Weichert J P and Counsell R E 2006 Synthesis and structure—activity relationship effects on the tumor avidity of radioiodinated phospholipid ether analogues *J. Med. Chem* **49** 2155–65

Riegel A C, Berson A M, Destian S, Ng T, Tena L B, Mitnick R J and Wong P S 2006 Variability of gross tumor volume delineation in head-and-neck cancer using CT and PET/CT fusion *Int. J. Radiat. Oncol. Biol. Phys.* **65** 726–32

Sanchez-Garcia M, Gardin I, Lebtahi R and Dieudonné A 2014 A new approach for dose calculation in targeted radionuclide therapy (TRT) based on collapsed cone superposition: validation with 90Y *Phys. Med. Biol.* **59** 4769

Schwartz D L, Ford E, Rajendran J, Yueh B, Coltrera M D, Virgin J, Anzai Y, Haynor D, Lewellyn B and Mattes D 2005 FDG-PET/CT imaging for preradiotherapy staging of head-and-neck squamous cell carcinoma *Int. J. Radiat. Oncol. Biol. Phys.* **61** 129–36

Sgouros G, Kolbert K S, Sheikh A, Pentlow K S, Mun E F, Barth A, Robbins R J and Larson S M 2004 Patient-specific dosimetry for 131I thyroid cancer therapy using 124I PET and 3-dimensional-internal dosimetry (3D-ID) software *J. Nucl. Med.* **45** 1366–72

Stabin M G 2008 Update: the case for patient-specific dosimetry in radionuclide therapy *Cancer Biother. Radiopharm.* **23** 273–84

Strigari L, Konijnenberg M, Chiesa C, Bardies M, Du Y, Gleisner K S, Lassmann M and Flux G 2014 The evidence base for the use of internal dosimetry in the clinical practice of molecular radiotherapy *Eur. J. Nucl. Med. Mol. Imaging* **41** 1976–88

Tomé W A and Fowler J F 2002 On cold spots in tumor subvolumes *Med. Phys.* **29** 1590–8

Weber W, Carter Y, Abdel-Dayem H M and Sfakianakis G 1999 Assessment of pulmonary lesions with (18)F-fluorodeoxyglucose positron imaging using coincidence mode gamma cameras *J. Nucl. Med.* **40** 574

Weichert J P, Clark P A, Kandela I K, Vaccaro A M, Clarke W, Longino M A, Pinchuk A N, Farhoud M, Swanson K I and Floberg J M 2014 Alkylphosphocholine analogs for broad-spectrum cancer imaging and therapy *Sci. Trans. Med.* **6** 240ra75

Wen P Y, Macdonald D R, Reardon D A, Cloughesy T F, Sorensen A G, Galanis E, Degroot J, Wick W, Gilbert M R and Lassman A B 2010 Updated response assessment criteria for high-grade gliomas: response assessment in neuro-oncology working group *J. Clin. Oncol.* **28** 1963–72

Werner-Wasik M, Nelson A D, Choi W, Arai Y, Faulhaber P F, Kang P, Almeida F D, Xiao Y, Ohri N and Brockway K D 2012 What is the best way to contour lung tumors on PET scans? Multiobserver validation of a gradient-based method using a NSCLC digital PET phantom *Int. J. Radiat. Oncol. Biol. Phys.* **82** 1164–71

Witzig T E 2006 Radioimmunotherapy for B-cell non-Hodgkin lymphoma *Best Pract. Res. Clin. Haematol.* **19** 655–68

Zaidi H and El Naqa I 2010 PET-guided delineation of radiation therapy treatment volumes: a survey of image segmentation techniques *Eur. J. Nucl. Med. Mol. Imaging* **37** 2165–87

Zevalin 2013 Package Insert (Irvine, CA: Spectrum Pharmaceuticals)

Zhu T, Hu R, Qiu X, Taylor M, Tso Y, Yiannoutsos C, Navia B, Mori S, Ekholm S and Schifitto G 2011 Quantification of accuracy and precision of multi-center DTI measurements: a diffusion phantom and human brain study *Neuroimage* **56** 1398–411